Engineering Applications of Artificial Intelligence 162 (2025) 112560

Contents lists available at ScienceDirect

Engineering Applications of Artificial Intelligence

journal homepage: www.elsevier.com/locate/engappai

Mechanical properties prediction of Bi-metal foam sandwiches using machine learning methods and elastic deformation behaviour

Mohammad Reza Chalak Qazani [a,b,*], Mohsen Dorudgar [c], Mehdi Moayyedian [d], Abdel-Hamid I. Mourad [e], Moosa Sajed [f], S.M. Hossein Seyedkashi [c], Siamak Pedrammehr [g]

[a] Colleger of Science and Engineering, James Cook University, Townsville, QLD 4815, Australia
[b] Faculty of Computing and Information Technology, Sohar University, Sohar, Sohar, 311, Oman
[c] Mechanical Engineering Department, University of Birjand, Birjand, 97175-376, Iran
[d] College of Engineering and Technology, American University of the Middle East, Kuwait
[e] Mechanical and Aerospace Engineering Department, College of Engineering, United Arab Emirates University, P.O. Box, Al Ain, 15551, United Arab Emirates
[f] Mechanical Engineering Department, Azarbaijan Shahid Madani University, Tabriz, Iran
[g] Faculty of Design, Tabriz Islamic Art University, Tabriz, Iran

ARTICLE INFO

Keywords:
Bi-metal sandwiches
Mechanical properties estimation
Application of artificial intelligence
Feedforward neural network
Long-short term memory
Genetic algorithm

ABSTRACT

Metal foam sandwiches are a kind of ultra-lightweight material made from a porous metal core bonded to two face sheets. Friction stir welding (FSW) is utilised in welding bimetal foam sandwiches. It is worth mentioning that the exact relation between mechanical properties and process parameters is challenging to determine. The innovation lies in the non-destructive estimation of mechanical properties (Young's modulus, ultimate tensile strength and fracture strain) through elastic deformation data and the novel application of artificial intelligence techniques optimised by genetic algorithms, eliminating dependency on input process parameters. After proper network training, three methods are employed to estimate these mechanical properties: a decision tree, a feedforward neural network and long-short term memory. These are chosen to investigate the influence of both machine/deep learning methods in predicting the mechanical properties of the FSW final product. Moreover, a genetic algorithm is employed to find the optimal hyperparameters of the three investigated prediction models to reach the highest accuracy. The results prove the efficiency of the proposed feedforward neural network in the estimation of Young's modulus and ultimate tensile strength for the bi-metal foam sandwiches with lower mean absolute error (MAE) and higher correlation coefficient compared to the decision tree (63.9 % lower MAE and 25.50 % higher correlation coefficient) and long-short term memory (77.50 % lower MAE and 25.05 % higher correlation coefficient). In addition, the proposed decision tree model accurately predicts the fracture strain with R-square and root mean square error as 0.61429 and 1.3862×10^{-5}, respectively.

1. Introduction

The aluminium foam sandwich comprises two metallic face sheets and a porous aluminium core bonded on both sides (Banhart et al., 2008). This structure provides peculiar properties, including strength, dimensional stability, impact resistance, and acoustic insulation in metallic foam sandwiches (García-Moreno, 2016). These sandwiches have special advantages compared to dense materials and pure foams, including a higher strength than a metallic sheet of the same mass. Also, compared to pure foam, their major advantage is that the outer face sheets allow the sandwich to tolerate higher tensile stresses (for example, when the panel is bent). A collection of these unique properties has made these panel sandwiches widely applied in the transportation, shipbuilding, railway, and aerospace industries (Banhart et al., 2012).

Adhesive bonding is one of the simplest and cheapest production methods of metallic foam sandwiches (Müssig et al., 2021). However, a few issues have restricted its application, including low strength, lack of thermal resistance, recyclability issues, and environmental concerns (Hangai et al., 2014; Brockmann et al., 2009). Another common method is soldering, especially for lightweight sandwich panels with a honeycomb structure (Zhang et al., 2020). Several other methods exist, such as foaming powder mixture, arc, tungsten inert gas (TIG), and laser welding. Nowacki et al. (2015) evaluated an Al-Si alloyed foam and an AlSi–SiC foam composite via TIG and laser welding techniques.

* Corresponding author. Institute for Intelligent Systems Research and Innovation, Deakin University, Geelong, VIC, 3216, Australia.
E-mail addresses: m.r.chalakqazani@gmail.com, mohamadreza.chalakqazani@jcu.edu.au (M.R. Chalak Qazani).

https://doi.org/10.1016/j.engappai.2025.112560
Received 31 August 2022; Received in revised form 2 February 2025; Accepted 29 September 2025
Available online 3 October 2025

Eventually, the welded joint structures were evaluated, and a higher tensile strength was obtained for the samples than the base metal. Yao et al. (2019) investigated the joint structure and strength of an aluminium foam sandwich produced via liquid diffusion welding. The method showed higher fracture and fatigue strengths compared to adhesive bonding. Various tests were conducted, and results were compared to joints made by adhesive bonding and soldering techniques. On the other hand, friction stir welding (FSW) uses a combination of friction-induced mechanical and thermal effects to connect the parts under the melting point of the parent material as a solid-state welding process (Geiger et al., 2008; Yang et al., 2008). FSW requires fewer facilities and low energy consumption compared to other welding methods. The applied tool for this process is an inconsumable cylindrical device with a pin on the joint boundary of two pieces. It connects them by applying a rotational movement, moving toward welding, and eventually by the material softening and flowing (Woo et al., 2008). Overlap joints from dissimilar alloys could be successfully produced using the FSW process. At the same time, it is limited to using other welding processes. On the other hand, foaming and welding could be achieved simultaneously, even for dissimilar alloys (Hangai et al., 2012). Hangai et al. (2014) used FSW to produce foam sandwiches. The process involved integrating ADC12 alloy parts with Al_2O_3 powder on an ADC6 aluminium alloy base. The resulting sample was a panelled sandwich with an aluminium foam core.

Researchers have been attracted to advancements in artificial intelligence for mapping complex and nonlinear data in various research fields, such as manufacturing, inorganic nanomaterials, energy, and material microstructure (Wu et al., 2022; Elsheikh, 2023; Rezaee et al., 2007; Kadkhodaie Ilkhchi et al., 2006). Although these data-driven systems are not reliant on the physics of the procedure, they can generate models with a higher precision level than classical mechanistic models (Ghanbari et al., 2022). Kruger et al. (2003) utilised a fuzzy logic controller unit to monitor and control FSW, eliminating operator dependence and enhancing manufacturing productivity and quality. Okuyucu et al. (2007) developed an artificial neural network (NN) model, specifically a feedforward NN, to analyse and simulate the correlation between FSW parameters and the mechanical properties of aluminium plates. Their model demonstrated good performance in accurately calculating mechanical properties. However, its reliance on input parameters may limit its generalizability beyond the specific studied conditions. Yousif et al. (2008) also employed a feedforward NN model to analyse and simulate the correlation between the FSW parameters of aluminium plates and their mechanical properties. The model's input parameters were traverse speed and tool rotational speed (TRS). In contrast, the output parameters were tensile strength, yield strength, and elongation. The selection and representation of the input parameters present a challenge, assuming they are the main factors influencing the mechanical properties. Furthermore, using simulated annealing techniques to prevent the network from getting trapped in local minima suggests that the optimisation process can be complex and computationally intensive. Mishra (2020) aimed to optimise the FSW process for maximum ultimate tensile strength (UTS) using a feedforward NN and decision tree (DT). He concluded that the feedforward NN yielded better and more accurate results than the DT. Eren et al. (2021) reviewed and evaluated various artificial intelligence techniques, including feedforward NN, fuzzy logic, machine learning, meta-heuristic methods, and hybrid systems, for FSW. They highlighted their contribution in determining optimal input parameters to achieve desired output parameters in different material combinations. Senapati et al. (2021) investigated the influence of FSW process parameters on microstructure and mechanical characteristics using a feedforward NN trained by Levenberg-Marquardt for optimisation in the automotive industry. Ghanbari and Mahmoudi (Ghanbari et al., 2022) implemented supervised machine learning with the k-nearest neighbours algorithm to estimate residual surface stresses and mechanical properties of materials. Nejad et al. (2022) proposed a surrogate model for AA2024-T351 aluminium alloy produced by FSW using a feedforward NN, with TRS and traverse speed as inputs and fatigue crack growth rate and fracture toughness as outputs. They employed multi-objective optimisation (NSGA-II) to select the optimal input parameters.

Recently, Elsheikh (2023) provided a comprehensive review of machine learning applications in FSW, encompassing prediction, integration with finite element methods, real-time control, tool failure diagnosis, and optimisation techniques. Elsheikh discovered that machine learning methods exhibit promising results in modelling various FSW processes, surpassing conventional statistical methods albeit with slightly higher computational time. Kumar et al. (2023) investigated the effect of different TRSs on force-torque, mechanical properties, and microstructure in FSW of Al-Cu-Li alloy plates, validating the results using a feedforward NN. Mishra (2023) examined several machine learning methods, including DTs, XGBoost, feedforward NN, random forests, gradient boosting, and AdaBoost, to predict the UTS of FSW magnesium joints, revealing that the XGBoost algorithm achieved the highest coefficient of determination. Table 1 shows the following articles on implementing artificial intelligence in FSW, including the investigated applications, main contribution and challenges.

The focus point of the previous studies (Elsheikh, 2023; Ghanbari et al., 2022; Kruger et al., 2003; Okuyucu et al., 2007; Yousif et al., 2008; Mishra, 2020, 2023; Eren et al., 2021; Senapati et al., 2021; Nejad et al., 2022; Kumar et al., 2023) for extracting the mechanical behaviour of the FSW products can be categorised into main groups. The first group of studies uses the tensile test to extract the mechanical behaviour of the FSW products. In contrast, the final product should be strengthened until the breakpoint. The second group focuses on extracting the mechanical based on the process parameters, including TRS, traverse speed, tilt angle, etc. However, both groups suffer from shortcomings. In the first group, the tensile test is destructive and cannot be used for all sandwiches produced in the production line. In the second group, the FSW process is very complicated, and it is impossible to consider all the parameters influencing the mechanical behaviour of the final product. Then, the process should be redeveloped in case of changing the process.

Our study innovatively employs machine learning and deep learning models (DT, NN, and LSTM) combined with GA optimisation to predict mechanical properties based on elastic deformation data. This approach eliminates the need for destructive testing. It overcomes the limitations of relying on specific input process parameters, which restrict the generalizability of conventional methods. This is the first study to explore the combined use of DT, NN, and LSTM for predicting mechanical properties based on the elastic deformation segment of stress-strain data, avoiding material destruction or parameter dependency. These innovations extend the applicability of these techniques to a wide range of materials and processes. In the following, the machine/deep learning methods have been exploited in this research to predict the mechanical properties of bi-metal foam sandwiches based on the elastic deformation behaviour without entering the plastic part, which changes the material's mechanical properties or destroys the final product. The dataset (training and testing) for the investigated supervised machine learning methods is gathered using 63 samples. The extracted results of 57 samples are selected for training and validation purposes of the investigated method. In comparison, 6 samples are chosen for testing purposes to practically evaluate the effectiveness of the proposed method. The tensile behaviours of the bi-metal foam sandwich are captured using the standard tensile test. Then, the mechanical properties of the sandwiches, including Young's modulus (E), UTS and fracture strain (FS), can be captured based on the curve. The supplementary material explains the process of extracting the E, UTS, and FS based on the captured plot of the standard tensile test. The feedforward NN, LSTM, and DT are employed to estimate the sandwiches' E, UTS, and FS based on their elastic deformation behaviour, which is expected not to destroy the plates. DT is a supervised machine learning algorithm used to classify or regress. It should be noted that DT is considered the traditional machine learning method that reaches the highest efficiency

Table 1
Review of articles on the implementation of artificial intelligence in FSW.

No	Author (Year)	Applications	Contribution	Challenges
1	Kruger et al. (Kruger et al., 2003) (2003)	FLS	1. Development of FSW machine 2. Implementation of intelligent monitoring and control systems 3. Statistical analysis and intelligent process control	1. Data analysis and interpretation 2. Intelligent process control 3. Generalizability and adaptability
2	Okuyucu et al. (Okuyucu et al., 2007) (2007)	FFNN	1. Development of FFNN for correlating FSW parameters and mechanical properties of aluminium plates 2. Accurate Calculation and Simulation of Mechanical Properties	1. Data availability and quality 2. Complex correlations 3. Generalizability and adaptability 4. Optimisation of parameters
3	Yousif et al. (Yousif et al., 2008) (2008)	FFNN	1. ANN model correlates FSW parameters and properties 2. Simulated influence of FSW parameters 3. Validation with measured data achieved	1. Selection of appropriate optimisation algorithm 2. Correlation with elongation
4	Mishra (Mishra, 2020) (2020)	DT, FFNN	1. Implementing 2 machine learning algorithm 2. Performance comparison of algorithms	1. Feature selection and representation 2. Model selection and performance 3. Overfitting and generalisation
5	Eren et al. (Eren et al., 2021) (2021)	Review Paper (Machine Learning, NN, FLS, Artificial Intelligence)	1. Review and evaluation of artificial intelligence techniques in FSW 2. Identification of input and output parameters 3. Analysis of material combinations	–
6	Senapati et al. (Senapati et al., 2021) (2021)	FFNN	1. Investigation of process parameters 2. Parametric characterisation using feedforward NN 3. Optimal condition identification	1. Complex parameter interactions 2. Data availability and accuracy 3. Computational complexity
7	Ghanbari and Mahmoudi (Ghanbari et al., 2022) (2022)	KNN, Kriging, FFNN	1. Development of a portable indentation apparatus 2. Comparison of data interpretation methods 3. KNN provided more accurate results	1. Accuracy and precision 2. Data interpretation 3. Experimental validation
8	Nejad et al. (Nejad et al., 2022) (2022)	FFNN; NSGA-II	1. Multi-Objective optimisation and Sensitivity Analysis 2. Implementation of different FFNNs to reach the highest performance 3. Investigation of fracture behaviour and fatigue crack growth	1. Experimental challenges 2. Interpretability and validity of results 3. Optimisation complexity
9	Elsheikh (Elsheikh, 2023) (2023)	MLR; KNN; RF; GPR; FFNN; SVM; RBFNN; FLS; ANFIS	1. Prediction of joint properties 2. Analysis of commonly used ML models 3. Real-time control of the FSW Process 4. Tool failure diagnosis 5. Incorporation of metaheuristic optimisation techniques and ML methods	1. Complex relationship modelling 2. Computational resources and real-time implementation
10	Kumar et al. (Kumar et al., 2023) (2023)	FFNN	1 Investigation of TRS on Heat Generation and Force-Torque 2. Integration between ML and Finite Element Methods 3. Analysis of Frictional Heat Generation and Grain Size	1. Complex relationship between TRS and parameters 2. Optimisation complexity and computational intensity 3. Limited generalizability
11	Mishra (Mishra, 2023) (2023)	DT; XGBoost; FFNN; RF; Gradient Boosting; AdaBoost	1. Prediction of UTS 2. Evaluation of Six Supervised ML Algorithms 3. Assessment of Input Parameter Importance	1. Complex relationship modelling 2. Optimisation complexity and computational intensity 3. Limited generalizability 4. Feature importance and dimensionality

ANFIS: adaptive neuro-fuzzy inference system; DT: decision tree; FFNN: feedforward NN; FLS: fuzzy logic system; GPR: gaussian process regression; KNN: k-nearest neighbours; ML: machine learning; MLR: multi-linear regression; NSGA-II: nondominated sorting genetic algorithm II; RBFNN: radial basis function NN; RF: random forest; SVM: support vector machine; TRS: tool rotational speed.

for less complicated datasets. Also, feedforward NN is selected as the earliest and most accurate machine learning model using back-propagation (Mahmoud et al., 2023). In addition, LSTM was selected because of its capacity to maintain time-lag dependence when handling time-series signals (Ranawat et al., 2023). A stress-strain plot can be treated as a time-series signal, considering strain as time and stress as output. Then, LSTM is chosen to be evaluated. As the second main contribution of this study, a GA optimisation method is employed to calculate the optimal hyperparameters of the three investigated methods.

This paper has been organised as follows: The following Section presents an overview of the bi-metal foam, sandwiches with an

aluminium foam core, and copper face sheets. Section 3 presents the methodology, including the studied techniques (feedforward NN, LSTM, and DT) combined with the GA optimisation methods. The studied techniques are validated and verified using MATLAB software, and Section 4 reports and discuss the results. After examining the most noticeable results, Section 5 presents the conclusions.

2. Overview of foam sandwiches

Continuing the research of the authors (Dorudgar et al., 2021), 99.99 % pure copper sheets (ASTM B115-10) and aluminium foams with the dimensions of 50 × 100 (mm^2) were used to produce the sandwiches. Mechanical properties of copper were obtained using the ASTM E8-M standard tensile test. The aluminium foam density was 0.6 (g/cm^3). The copper sheet and aluminium foam thickness was 2 and 4 (mm), respectively. The ALPORAS aluminium foam was used as the core foam. These foams are anisotropic. Also, their minimum tensile and compressive strengths are in the through-thickness direction. Generally, these materials have a tensile behaviour similar to dense substances but have several peaks during compression (McCormack et al., 2001). A range of yield stresses is seen (Marx et al., 2021). The tool material has to be selected to show a high abrasion resistance and excellent high-temperature stability (Hangai et al., 2014). Thus, the tool was fabricated from hot-worked AISI H13 steel. The tool pin was designed with a cone shape frustum on a cylindrical base and was made by machining. Its hardness was increased to 52 Rockwell C by heat treatment. Fig. 1a–b shows the schematic representation and experimental setup of the bi-material sandwich plate production using FSW. Dimensions and the shape of the tool are shown in Fig. 1a.

Welding was accomplished by utilising a CNC milling machine. The aluminium foam in the middle of two copper face sheets was fixed on the table to avoid separating the sheets under high longitudinal forces applied to the parts during welding. The spindle axis was titled the vertical axis for a suitable connection. The tool was mounted to the spindle axis. After the device is turned on and the rotational motion of the spindle is started, the rotating tool pin penetrates the parts up to a depth of 4 (mm). The tool pin rotates statistically for 4 s in the same position to generate the necessary heat for the proper flow of materials at the beginning of the tool displacement. Then, the progressive movement of the table starts, and the tool pin moves directly by a length of 50 (mm). Then, the operator turns the specimen upside-down to weld the opposite side of the product. The process is schematically shown in Fig. 1a.

A constant progressive traverse speed of 20 (mm/min) was selected for welding. The different ranges of TRS and the tilt angle of the tool were studied. It has been observed that the apparent quality of the weld was not suitable at TRS below 2000 (rpm). Therefore, the TRS was studied between 2000 and 3000 (rpm). In addition, the different range of tilt angles has been investigated. It is observed that the angles below 5° lead to a good penetration depth. Then, these angles were ignored in the design of the experiment. So, the angles between 5°-7° were selected for the investigations.

It should be noted that 63 experiments were performed using the different ranges of the TRS (2000–3000 (rpm)), the tilt angle (5°-7°), and the fixed progressive traverse speed (20 (mm/min)). The experiment's full factorial design is chosen to generate the training/testing dataset with the highest accuracy. In addition, the six samples are chosen as the test sample to validate the proposed method in the point of accuracy via comparing the predicted value with the required value measured with tensile tests.

TRS and tilt angle are vital variables that impact joint mechanical properties. The rotational speed determines heat input during welding, with higher speeds resulting in increased input. A rotational speed below 1000 rpm is not recommended for optimal mixing and joining due to low heat input. In the case of overlap joints and thicker sheets, higher heat input (TRS) is required. In this study, considering sheet thickness and the brittle nature of aluminium foam, a minimum rotational speed of 2000 rpm is necessary, while the maximum is set at 3000 rpm to avoid poor microstructure. Tilt angle is crucial in material mixing and forging pressure during welding. Due to the chosen welding position, a higher tool tilt angle is necessary for proper material mixing, set at a minimum of 5°. However, excessively high tilt angles reduce joint strength, particularly concerning the upper sheet thickness. Therefore, the upper limit for the tilt angle is set at 7°. The samples were wire cut according to the determined dimensions in Fig. 1a. The prepared samples were examined using a Zwick/Roell Z600 tensile test machine with a maximum force of 600 (KN) and a traverse speed of 1 (mm/min). Also, Fig. 1b indicates the experimental setup of FSW for welding bi-metal foam sandwiches.

3. Methodology

This paper aims to estimate the E, UTS and FS of bi-metal foam sandwiches with aluminium foam core and copper face sheets based on the stress-strain behaviour of the plates. The employed data inside the NN model is obtained via tensile tests for the 63 produced samples. Unlike traditional applications, the current study leverages elastic deformation data from stress-strain plots as the sole input for predicting Young's modulus, ultimate tensile strength, and fracture strain. By utilising GA optimisation, the DT, NN, and LSTM hyperparameters are tailored for maximum predictive efficiency in this novel application.

Fig. 2a–b represents the schematic proposed model in this paper using three investigated models, from manufacturing bi-metal foam sandwiches to estimating E, UTS and FS. Based on Fig. 2a, the process

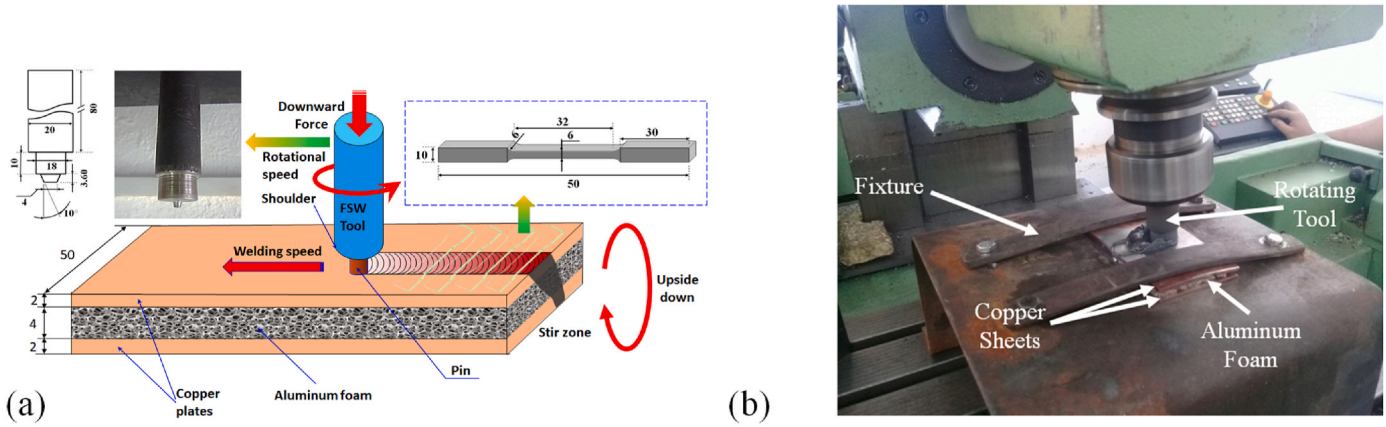

Fig. 1. Bi-material sandwich plate production using FSW and extraction of the tensile sample (a): The schematic representation (b): experimental setup.

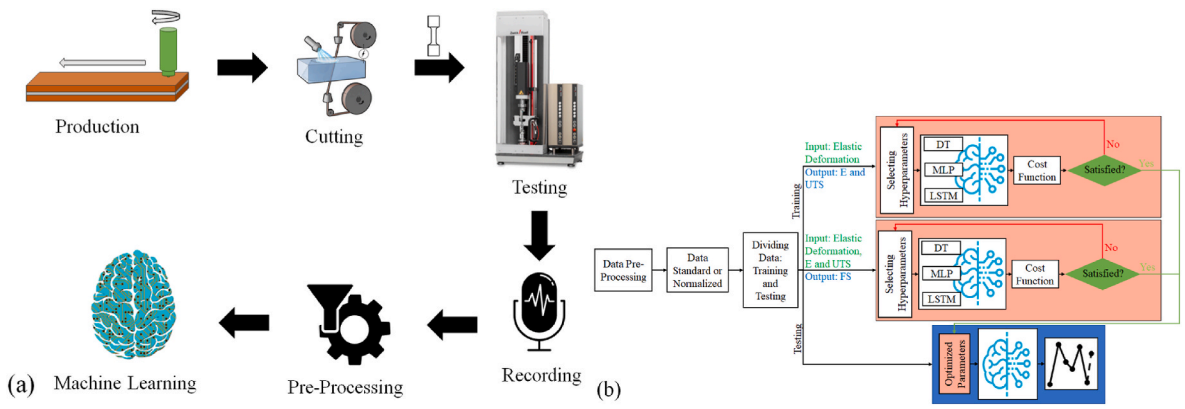

Fig. 2. (a): The schematic structure of the proposed method; (b): The artificial intelligence part of the study.

started with producing the bi-metal sandwiches made of aluminium foam core and copper face sheets using FSW. Then, a Wire electrical discharge machine is employed to cut the produced samples perpendicular to the welding line for tensile tests. The test results are recorded to be employed in the proposed model (EUTS-model) for estimating the E and UTS based on the elastic deformation of the sandwiches. In addition, FS-model is used to estimate the FS based on the elastic deformation of the plates and the calculated E and UTS by EUTS-model. Fig. 2b shows the implementation of the newly proposed DT, MLP and LSTM, which GA optimises on the stress-strain curves dataset. Two models need to calculate the requested parameters, including E, UTS, and FS, including the EUTS-model and FS-model. The input data for the models include the stress values corresponding to the elastic deformation range (0–0.0015 strain for all samples) extracted from the stress-strain plots obtained through tensile tests. For the EUTS-model, the outputs include E and UTS, where E is calculated as the slope of the stress-strain curve in the elastic region, and UTS is the peak stress. For the FS-model, the input includes elastic deformation data, along with the previously calculated E and UTS values, to predict fracture strain (FS), which is the elongation at the breaking point of the specimen. This relationship ensures that the prediction models leverage only non-destructive elastic deformation data, eliminating reliance on process parameters. In this regard, three machine/deep learning models are evaluated to calculate the outputs with higher efficiency, including DT, MLP, and LSTM. The algorithm is composed of data pre-processing for eliminating the duchy data to raise the algorithm's accuracy. Also, the Butterworth analogue filter is employed to filter the noise of the recorded stress-strain plot of the sandwiches to reach a higher accuracy via the proposed methods. Also, standardisation or normalisation is used to reduce the system's complexity for a network.

The GA evolutionary-based optimisation is employed to select the optimal DT, MLP and LSTM hyperparameters to reach the lowest means square error (MSE) between the predicted and actual data. It should be noted that there are two models, including EUTS-model and FS-model, for the prediction of E and UTS (using EUTS-model) and FS (using FS-model). After dividing the data into testing and training groups, the training data are used to train the model. In contrast, the testing data are used to test the model. Eventually, to compare the suggested models, the testing data are applied to the optimum extracted MLP, LSTM, and DT. Fig. 3 presents the stress-strain plot of the aforementioned 6 testing samples. It is the raw recorded data from the tensile test without filtering the signal using the Butterworth filter. The low-pass Butterworth filter with three filter orders and 9500 (rad/s) passband edge frequency is employed for filtering the recorded signals.

In addition, Table 2 represents the peaks of these six samples during the tensile strength test.

3.1. Pre-tuning of algorithm

Before model development and dataset application, three tasks

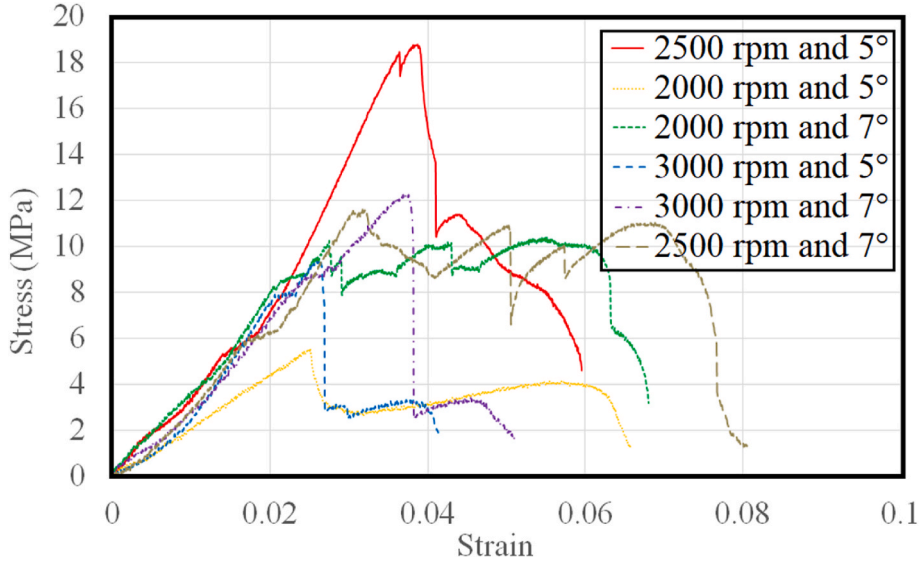

Fig. 3. The obtained dataset from the six-sample tensile test tests the proposed artificial intelligence methods (Dorudgar et al., 2021).

Table 2
The peaks of samples during the tensile strength test are used to test the algorithm.

No	First Peak		Second Peak		Third Peak		Fourth Peak	
	Stress	Strain	Stress	Strain	Stress	Strain	Stress	Strain
1	18.69	0.038	11.32	0.044	–	–	–	–
2	5.43	0.025	4.07	0.056	–	–	–	–
3	9.84	0.027	10.02	0.043	10.30	0.055	–	–
4	9.30	0.026	3.24	0.038	–	–	–	–
5	12.20	0.038	3.36	0.046	–	–	–	–
6	11.50	0.032	10.83	0.050	9.93	0.057	10.93	0.068

concerning the data should be completed. At first, the outlier data must be discarded because they are created due to faulty sensors. The second step is system standardisation or normalisation to reduce the system's data complexity before undergoing a training procedure. This paper employs both techniques in the system to decrease the complexity of the input data of the network and enhance the system's accuracy. One can use the Equation below to estimate the data standardisation:

$$\sigma_{x_i} = \frac{x_i - \overline{x}}{\sigma_x} \tag{1}$$

in which σ_{x_i} and x_i stand for the standardised and raw ith input data, respectively. In addition, σ_x and $\widetilde{x}$ are the functions for extracting the standard deviation and average of the data. The normalised data are determined by:

$$n_{x_i} = \frac{x_i - \underline{x}}{\overline{x} - \underline{x}} \tag{2}$$

in which n_{x_i} stands for the ith normalised input. In addition, $\underline{x}$ and $\overline{x}$ stand for the functions for extraction of the minimum and maximum datasets. During the final process of network pre-tuning, 90 % of the data is allocated to the network's training. In comparison, the remaining 10 % is dedicated to its testing. Due to the limited dataset size of 63 samples, we divided the dataset into two groups: 90 % for training (57 samples) and 10 % for testing (6 samples). A separate validation set was not employed to avoid further reducing the number of training samples, which could compromise the model's ability to learn effectively. To address the absence of a dedicated validation set, we utilised a leave-one-out cross-validation (LOOCV) approach during training. This approach involves iteratively training the model on all samples except one, the validation sample, and repeating this process for each sample in the training set. LOOCV ensures that the training process is robust and mitigates the risk of overfitting despite the limited dataset size.

The input signals of the EUTS-model are calculated based on the stress of the samples during the elastic deformation. It is the stress of the material during the 0–0.0015 strain of the samples. The outputs of EUTS-model are calculated based on the maximum stress of each plot to extract the UTS. Besides, the slope of the stress-strain plot in 0–0.01 strain is the E of each sample. The extracted E and UTS are the outputs of EUTS-model. The FS-model's inputs are the material's stress during the 0–0.0015 strain, calculated E via EUTS-model and UTS via EUTS-model. The output of the FS-model is FS, defined as the elongation at break or the ratio between the changed length concerning the initial length after breakage of the test specimen. Three models, including DT, NN, and LSTM, have been used in this paper for developing EUTS-model and FS-model to estimate the mechanical properties of the sandwiches.

3.2. Input-output relationship

The input data for the models include the stress values corresponding to the elastic deformation range (0–0.0015 strain for all samples) extracted from the stress-strain plots obtained through tensile tests. For the EUTS-model, the outputs include Young's modulus (E) and ultimate tensile strength (UTS), where E is calculated as the slope of the stress-strain curve in the elastic region, and UTS is the peak stress. For the FS-model, the input includes elastic deformation data, along with the previously calculated E and UTS values, to predict fracture strain (FS), which is the elongation at the breaking point of the specimen. This relationship ensures that the prediction models leverage only non-destructive elastic deformation data, eliminating reliance on process parameters.

3.3. Decision tree

DT is an expanded data mining technique with broad applicability in the analysis (van Diepen et al., 2006). It utilises leaf and branch nodes connected by decision pathways, defining decision boundaries through inequality expressions. By splitting data based on conditions, DT forms a binary tree and continues until reaching a leaf node for final predictions.

This paper employs the CART model, a nonparametric regression technique based on recursive partitioning. In order to train the appropriate DT, the information related to the elastic deformation of the specimen is defined as the algorithm's input via defining the E and UTS for the first model (EUTS-model as shown in Fig. 2b). Also, the elastic deformation of the specimen with a combination of already predicted E and UTS are defined as the inputs of the DT with selecting the FS as the system outputs for the second model (FS-model as shown in Fig. 2b). In addition, it should be noted that the input is the matrix based on the different stress and strain of the specimens during the elastic deformation in different intervals recorded via the stress-strain test machine. The hyperparameters of the DT are categorical predictors, minimum parent size and a maximum number of splits chosen based on GA evolutionary-based optimisation.

3.4. Feedforward neural network

The simplest NN consists of three layers: output, hidden, and input (Rosenblatt, 1957). Hidden and output layer neurons use nonlinear activation functions. The hidden layer can have multiple layers as needed. NN is used for supervised training in regression and classification problems. During training, inputs and outputs adjust network parameters (weights and biases) and minimise errors between predicted and target outputs. In this study, inputs are matrices representing stress and strain intervals, while outputs are E, UTS, and FS obtained from stress-strain plots for each sample. The backpropagation algorithm optimises weights and biases based on RMSE or MSE.

In the context of NN training, the stochastic gradient descent method is employed to adjust biases and weights during the backward pass of the network. During training, the jth output node in the nth data point can be expressed as the difference between the actual output ($\boldsymbol{T}$) and the target output ($\widehat{\boldsymbol{T}}$). Weight adjustments are made to minimise the network's error, which involves calculating the gradient of the error concerning the weights. The gradient descent technique determines how weights change, where the learning rate (η) is crucial in ensuring convergence. The derivative of the activation function and the error are involved for output nodes, while for hidden nodes, the weight derivatives depend on the weights of the output layer and the activation function's derivative. This process, known as backpropagation, enables the adjustment of weights in both hidden and output layers based on the

derivative of the activation function, facilitating the neural network's learning. The hyperparameters of the NN are the number of layers, number of neurons and mutation, which are selected based on GA evolutionary-based optimisation in the last subsection.

3.5. Long-short term memory

Hochreiter and Schmidhuber (Hochreiter et al., 1997) demonstrated the effectiveness of LSTM in handling time lag dependence in recurrent NNs. The LSTM model uses memory blocks to process long data sequences. The output is generated through a regression layer and a fully connected layer. Inputs and outputs in the training process are defined based on recorded stress-strain plots of bi-metal foam sandwiches produced via FSW.

LSTM models employ forget, input, and output gates, which use various functions and products to manage data flow and retain gradient information. These gates help preserve valuable historical information while updating memory units and enhancing learning. Inputs represent stress and strain data from a stress-strain test machine, and outputs are combinations of E, UTS, and FS for each tested sample. The memory cell at each time step, $\boldsymbol{c}_t^j$, gets updated by integrating a new value, $\tilde{\boldsymbol{c}}_t^j$, while forgetting outdated data using the forget gate, $\boldsymbol{f}_t^j$. The input gate, $\boldsymbol{i}_t^j$, and output gate, $\boldsymbol{o}_t^j$, are responsible for deciding which information is propagated, all within the [0, 1] range. The final output, y, is generated using a centred logistic sigmoid function. Training involves truncated backpropagation and real-time recurrent learning through time with gradient descent optimisation, minimising the loss function and improving memory cell performance. The LSTM hyperparameters include the number of units, learning rate, and layers selected based on the GA evolutionary-based optimisation in the following subsection.

3.6. Genetic algorithm

Michelle (Mitchell, 1998) introduced GA inspired by genetic systems' natural selection. The first stage involves the random selection of the population from chromosomes. The fitness function evaluates the extracted chromosomes. GAs accommodate complex objective functions, search for global optima, explore diverse solutions, tolerate noisy environments, and optimise discrete variables. When facing non-differentiability, global optimisation, exploration-exploitation trade-offs, noise, or combinatorial problems, GAs are the preferred choice.

To improve the accuracy and convergence speed of the solution, it is crucial to select the parameters of the GA carefully. The appropriate configuration of mutation rates and crossover settings ensures the success of the GA and the extraction of reliable results (Lin et al., 2003). A high mutation rate increases the risk of overlooking the solution. In contrast, a low mutation rate can lead to getting stuck in a local optimum. In this study, a population size of 80 was chosen. A smaller population limits the GA's search capability. A larger population only increases optimisation time without noticeable improvement in results. The obtained results of the GA demonstrate the suitable selection of parameters, including crossover friction, mutation rate, generation, and population, for addressing the problem. Table 3 shows the adjustments of GA.

Table 3
GA Adjustment Parameters for machine learning methods hyperparameters.

Parameters	Value
Number of Hyperparameters	3
Maximum Generation	500
Population Size	80
Function Tolerance	10^{-6}
Crossover Rate	0.8
Mutation Function	Adaptive Feasible

Finally, three proposed models, including DT, NN and LSTM, were modelled in MATLAB. They were tuned using GA. Then, they were compared to extract the more efficient model in estimating E, UTS and FS via the proposed EUTS-model and FS-model.

3.7. Validation

Five parameters have been used in this paper to validate the proposed method compared with traditional methods, including correlation coefficient (CC), mean absolute error (MAE), MSE, RMSE, and R-square. These validation parameters are calculated as follows:

$$\mathrm{CC} = \frac{\sum_{i=1}^{n}(x_i - \overline{x})(T_i - \overline{T})}{\sqrt{\sum_{i=1}^{n}(x_i - \overline{x})^2 (T_i - \overline{T})^2}} \tag{17.a}$$

$$\mathrm{MAE} = \frac{\sum_{i=1}^{n}|T_i - \widehat{T}_i|}{n} \tag{17.b1}$$

$$\mathrm{MSE} = \frac{1}{n}\sum_{i=1}^{n}(T_i - \widehat{T}_i)^2 \tag{17.b2}$$

$$\mathrm{RMSE} = \sqrt{\frac{\sum_{i=1}^{n}(T_i - \widehat{T}_i)^2}{n}} \tag{17.c}$$

$$\mathrm{R}^2 = 1 - \frac{\sum (T_i - \widehat{T}_i)^2}{\sum (T_i - \overline{T})^2} \tag{17.d}$$

in which $\boldsymbol{x_i}$, $\boldsymbol{n}$, $\boldsymbol{T_i}$, $\overline{\boldsymbol{x}}$, $\widehat{\boldsymbol{T}}_{\boldsymbol{i}}$, and $\overline{\boldsymbol{T}}$ stand for the ith input, the number of samples, ith output, the mean of inputs, the ith predicted value and the mean of outputs.

4. Results and discussions

Initially, the stress-strain diagram (Fig. 3) is explained in this Section. Then, three investigated models in Section 3, combined with the GA optimisation method, are coded in MATLAB. DT is developed based on the explained model in Section 3.2. NN is prepared based on the presented model in Section 3.3. Besides, the LSTM is prepared based on the presented mathematical model in Section 3.4. Lastly, three models are optimised based on the GA optimisation method presented in Section 3.5.

According to the stress-strain diagram depicted in Fig. 3, no specific oscillation is observed in the first test until reaching the yield stress, indicating the homogeneity of the aluminium foam-to-copper weld joint in this sample. However, in the third sample, it can be observed that the diagram is almost linear up to a stress of 0.8 MPa. However, significant fluctuations occur due to the porosity of the aluminium foam, leading to the formation of an inhomogeneous weld joint. In the sixth test, until reaching the ultimate stress, the diagram maintains a constant slope, with only one oscillation observed at a stress of 6 MPa. However, after surpassing the ultimate stress with a value of 11.6 MPa, the diagram exhibits numerous fluctuations, indicating the inhomogeneity of the weld joint due to the porosity of the aluminium foam caused by the high rotational speed of the tool. It is observed that the stress-strain diagrams of the samples at rotational speeds of 2000 and 2500 rpm are similar to the monolithic piece. However, at a rotational speed of 3000 rpm, the stress-strain diagram exhibits significant fluctuations due to the lack of formation of a uniform structure, ultimately resulting in the formation of an inhomogeneous weld joint due to the high rotational speed of the tool. With a deviation angle of 5°, increasing the rotational speed of the

tool reduces initially and then increases the tensile strength. However, the maximum strength is associated with the sample welded at the lowest tool speed. The decrease in tensile strength is mainly caused by forming internal voids and creating micro-cracks in the weld structure. The sample welded at 2000 rpm, with a 5-degree deviation angle, has a higher strength, while the conditions are reversed in the two higher speeds. Overall, within the studied range, it can be concluded that the rotational speed of the tool has a more significant effect than the deviation angle, and increasing the deviation angle, considering the increased penetration depth, leads to improved strength.

Regarding the samples welded at 2000 rpm, which deviate from this trend, it seems that the asymmetric porosity of the foam in the tested region could be the reason for this difference. As mentioned earlier, the highest tensile strength is related to Sample 1, with a value of 18.8 MPa. Lower rotational speed and smaller deviation angle of the tool result in more balanced pressure and lower temperature during welding compared to the other samples. The lowest tensile strength is associated with the samples welded at higher rotational speeds of the tool, namely 2500 and 3000 rpm. Therefore, it can be said that this result might be due to higher heat generated during welding caused by the higher rotational speed of the tool, which leads to the formation of a region affected by higher heat, a less cohesive structure, small cracks, and other defects.

MATLAB software's fitrtree, feedforwardnet and trainNetwork functions are used to design the DT, NN and LSTM models. The results are interpreted using the plot function. Besides, the GA method is developed using the ga function. In order to prevent the system from overfitting problems, a leave-one-out cross-validation methodology is employed to do the cross-validation of the networks during the training process. One sample and performance are evaluated on the left-out sample. It was performed for each of the 10 samples in the dataset.

The GA optimisation method calculates the optimal hyperparameters of the proposed DT, NN and LSTM. Table 4 shows the optimised hyperparameters of the proposed DT, NN and LSTM using GA inside EUTS-model and FS-model.

The GA optimisation method's convergence plot for calculating the optimised EUTS-model hyperparameters using DT, NN and LSTM is reported in Fig. 4a–c, respectively. In addition, the GA optimisation method's convergence plot for calculating the optimised FS-model hyperparameters using DT, NN and LSTM is reported in Fig. 5a–c, respectively. The EUTS-model estimates E and UTS based on the elastic deformation part of the tensile-extension plot. Also, FS-model is used to estimate the FS based on the elastic deformation of the samples as well as the recalculated E and UTS of the sample via EUTS-model.

Table 4
The extracted DT, NN, and LSTM hyperparameters were used using the GA optimisation method for the EUTS-model and the FS-model.

Methods	Machine Learning	Number of categorical predictors or layers	Number of minimum parent size or neurons or units	Maximum number of splits or mutation or learning rate
EUTS-model	DT	Number of categorical predictors: 3	Number of minimum parent size: 20	Maximum number of splits: 24
	Feedforward NN	Layers: 4	Neurons: 348	Mutation rate: 0.0015
	LSTM	Layers: 2	Units: 232	Learning rate: 0.9861
FS-model	DT	Number of categorical predictors: 1	Number of minimum parent sizes: 26	Maximum number of splits: 7
	Feedforward NN	Layers: 18	Neurons: 23	Mutation rate: 0.0005
	LSTM	Layers: 2	Units: 215	Learning rate: 0.4144

FS-model and EUTS-model are trained and tested using three investigated models to estimate the E, UTS, and FS. The polar error histogram of feedforward NN and LSTM during the training and testing process for calculation of the UTS are shown in Fig. 6a–b, respectively. Based on the represented results in Fig. 6a, the mean of the error using feedforward NN to calculate UTS by implementing all datasets (training and testing) is 8.53×10^{-4}. It should be noted that the average error during the training and testing are -2.7×10^{-3} and 3.48×10^{-2}, respectively. The variation of the error in calculating the UTS under the feedforward NN model using both training and testing datasets is 0.4065. The error variation 0.4147 and 0.3488 of the error variation correspond to the training and testing process. Also, Fig. 6b shows that the mean and variation of the error using LSTM to calculate UTS with the implementation of all datasets (training and testing) are 0.6913 and 0.4713, respectively.

Fig. 7a–b shows the regression of the data during the testing and training procedures for the calculation of FS under feedforward NN and LSTM, respectively. Based on the represented results in Fig. 7a, the R^2 between the actual and predicted FS using feedforward NN for all datasets (training and testing) is 0.9999. Fig. 7b presents that the R^2 between the actual and predicted FS using LSTM for all datasets (training and testing) is −20.35. In addition, the R^2 between the actual and predicted FS for training and testing datasets using feedforward NN are 0.9999 and 0.9991. It is reported that −19.3302 and 0.0117 for LSTM during training and testing, respectively. The negative value on R^2 using the LSTM method (Fig. 7b) proves the inefficiency of this investigated method in extracting the FS because the prediction is worse than a constant function that always predicts the mean of the data.

To quantitatively analyse the relationships between inputs and outputs, Pearson CC were computed to evaluate the linear dependency between the elastic deformation features and the target outputs (E, UTS, FS). The results indicate a strong positive correlation between the elastic deformation data and E and UTS (CCs: 0.92 and 0.88, respectively). At the same time, FS demonstrates a moderate CC of 0.72 due to the complex nonlinear dependency. These findings highlight the suitability of the proposed inputs for accurately predicting the mechanical properties.

The results obtained in the testing procedures of the three studied techniques are shown in Table 5, according to which LSTM is regarded as the weakest algorithm during the data testing stage because it is a EUTS-model with the maximum number of errors. The MSE between the actual and predicted UTS and E using LSTM are 0.663 and 210.7481. On the other hand, NN is the most accurate candidate for EUTS-model in the prediction of UTS and E based on the elastic deformation of the sandwiches with MSE of 0.10262 and 2.7746, respectively. Besides, DT is the most accurate model for calculating FS based on the sandwiches' elastic deformation. UTS and E. LSTM cannot reach reasonable results as the FS-model is the same as the EUTS-model. It is worth mentioning that CC is a statistical metric and should be followed by a statistical test or confirmation parameter like "P-value".

The graphical representation of Table 5 is shown in Fig. 8. Fig. 8a–c shows the actual and predicted E, UTS and FS of the testing samples (6 testing samples) using three investigated methods, respectively. Based on the represented results in Fig. 8a, the CC between the actual and predicted E using optimised DT, NN and LSTM are 0.51429, 0.98571 and 0.58571, respectively. It proves the efficiency of optimised NN in handling the prediction of E as EUTS-model. Based on Fig. 8b, the CC between the actual and predicted UTS using optimised DT, NN, and LSTM are 0.87143, 0.9 and 0.81429, respectively. It proves the efficiency of optimised NN in handling the prediction of UTS as EUTS-model. Lastly, Fig. 8c shows that CC between the actual and predicted FS using optimised DT, NN, and LSTM are 0.61429, 0.37143 and 0.2, respectively. It proves optimised DT's efficiency in handling the FS prediction as an FS-model.

Fig. 9a–c represents the error between the actual and predicted E, UTS and FS of the testing dataset (6 testing samples) using three

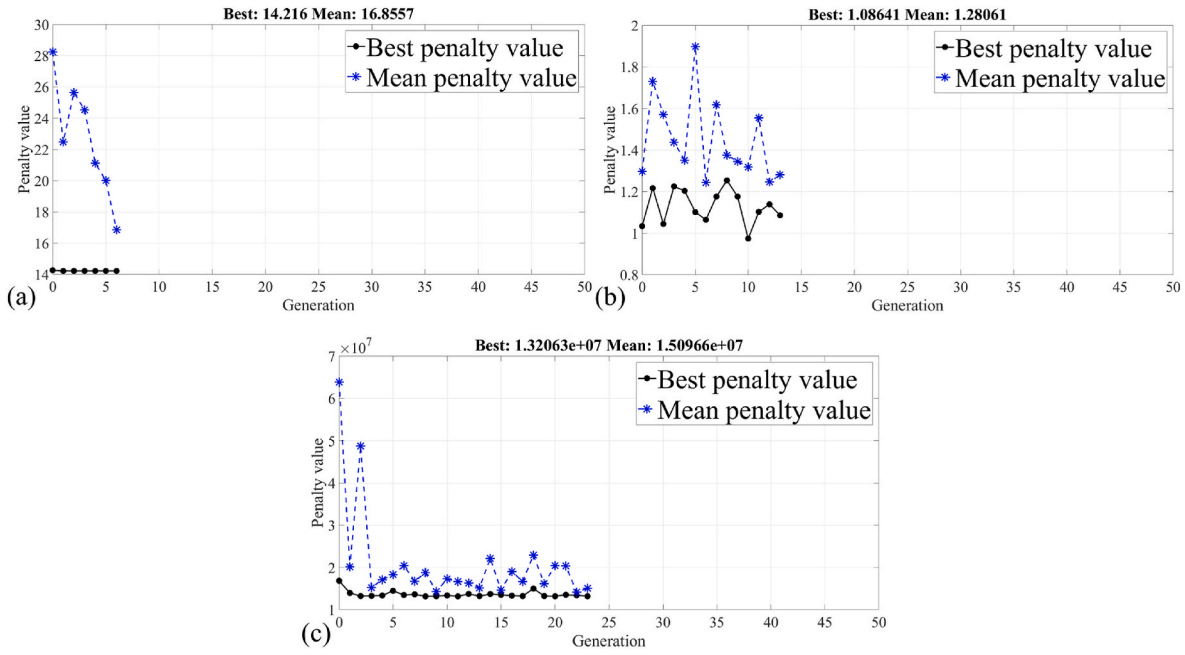

Fig. 4. The convergence plot of GA optimisation method in the development of EUTS-model for estimation of E and UTS based on the elastic deformation of the sandwiches in (a): DT; (b): NN; (c): LSTM.

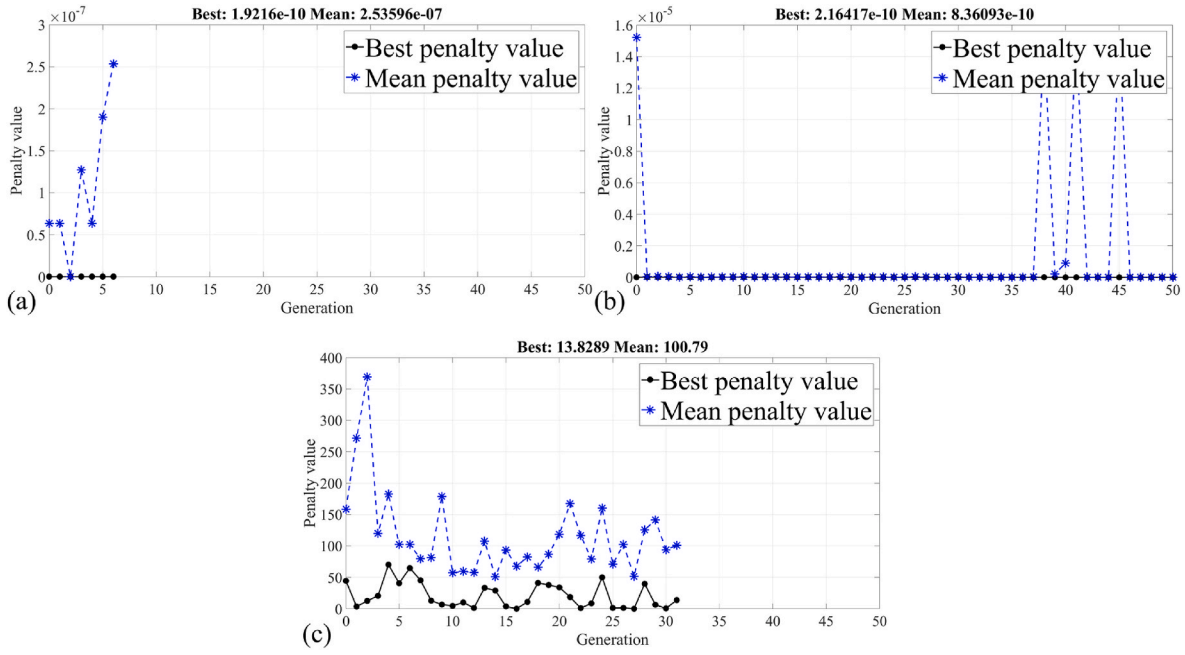

Fig. 5. The convergence plot of GA optimisation method in the development of FS-model for estimation of FS based on the elastic deformation of the sandwiches in (a): DT; (b): NN; (c): LSTM.

investigated methods, including optimised DT, NN and LSTM, respectively. Based on the results represented in Fig. 9a–b, it is obvious that NN is the best EUTS model for predicting E and UTS in points with less RMSE. In addition, Fig. 9c proves that the optimised DT is the best FS-model for predicting FS with the least RMSE.

The results presented in this Section prove the efficiency of the newly proposed optimised NN as EUTS-model and optimised DT as FS-model compared with other investigated models in terms of higher CC and R-square and lower MSE, RMSE and MAE.

5. Conclusion

This study investigates a new NN model to estimate bi-metal foam sandwiches' E, UTS, and FS. These sandwiches consist of an aluminium foam core and copper face sheets, and their mechanical properties are typically assessed through destructive testing. This study aims to develop a non-destructive model that can accurately calculate the mechanical properties of the sandwiches using elastic deformation data. To achieve this, 63 samples were produced with varying production parameters, such as TRS and tilt angle. All 63 samples underwent standard tensile testing, generating stress-strain plots. The dataset was divided,

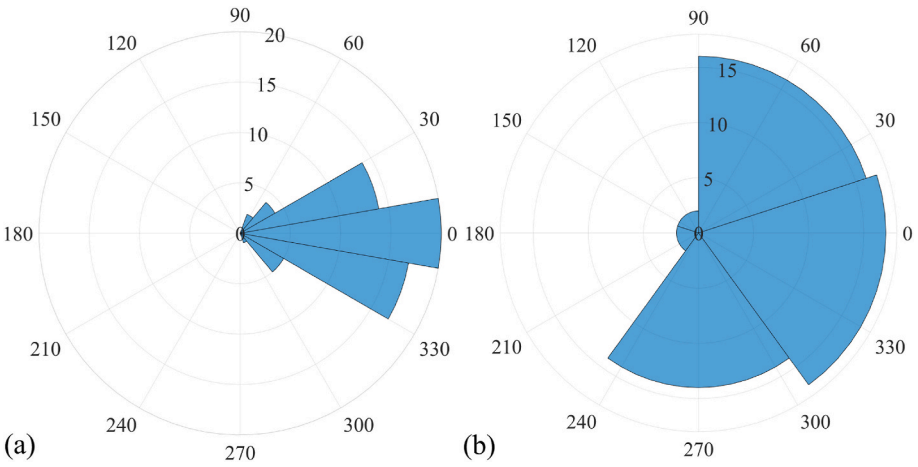

Fig. 6. The polar error histogram of the data during the testing and training procedures for calculating UTS under (a) feedforward NN; (b) LSTM.

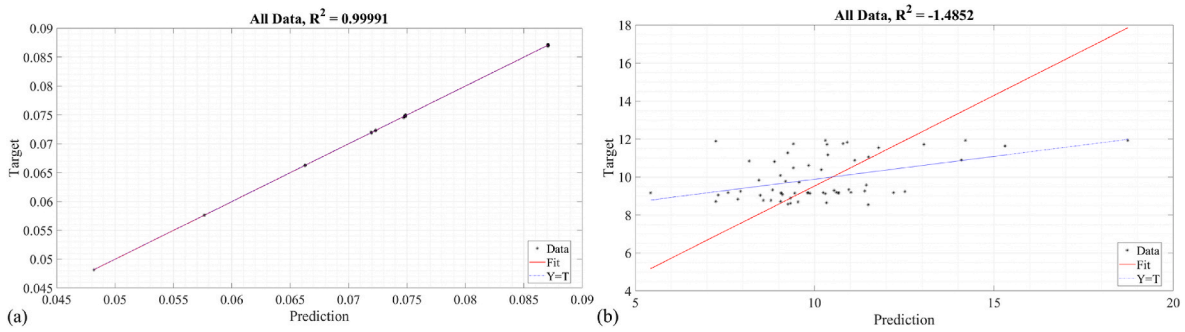

Fig. 7. The regression of the data during the testing and training procedures for calculation of FS under (a) feedforward NN; (b) LSTM.

Table 5
The results of DT, NN and LSTM were extracted using the GA optimisation method for EUTS-model and FS-model.

Output	Method	Mean Error	Std Error	MSE	RMSE	MAE	MAPE	CC	R^2
EUTS-model	DT-UTS	2.89×10^{-1}	5.44×10^{-1}	3.30×10^{-1}	5.74×10^{-1}	5.02×10^{-1}	5.2782	8.71×10^{-1}	6.28×10^{-1}
	DT-E	−1.43	5.59	2.81×10^{1}	5.30	4.83	1.7598	5.15×10^{-1}	-inf
	NN -UTS	$\mathbf{3.48 \times 10^{-2}}$	$\mathbf{3.49 \times 10^{-1}}$	$\mathbf{1.03 \times 10^{-1}}$	$\mathbf{3.20 \times 10^{-1}}$	$\mathbf{2.63 \times 10^{-1}}$	**2.8199**	$\mathbf{9.00 \times 10^{-1}}$	
	NN -E	$\mathbf{-0.6{,}93 \times 10^{-1}}$	**1.66**	**2.77**	**1.67**	$\mathbf{0.9.64 \times 10^{-1}}$	**0.3521**	$\mathbf{9.86 \times 10^{-1}}$	$\mathbf{8.95 \times 10^{-1}}$
	LSTM-UTS	$\mathbf{6.91 \times 10^{-1}}$	$\mathbf{4.71 \times 10^{-1}}$	$\mathbf{6.63 \times 10^{-1}}$	$\mathbf{8.14 \times 10^{-1}}$	$\mathbf{0.6.91 \times 10^{-1}}$	**7.5701**	$\mathbf{0.8.14 \times 10^{-1}}$	**−4.66**
	LSTM-E	1.37×10^{1}	5.29	2.11×10^{2}	1.45×10^{1}	1.37×10^{1}	5.2728	5.86×10^{-1}	-1.01×10^{2}
FS-model	**DT**	$\mathbf{9.6 \times 10^{-6}}$	$\mathbf{1.10 \times 10^{-5}}$	$\mathbf{1.92 \times 10^{-10}}$	$\mathbf{1.39 \times 10^{-5}}$	$\mathbf{1.00 \times 10^{-5}}$	**0.0115**	$\mathbf{6.14 \times 10^{-1}}$	**-inf**
	NN	3.25×10^{-5}	3.76×10^{-5}	2.23×10^{-9}	4.73×10^{-5}	4.69×10^{-5}	0.0538	3.71×10^{-1}	-3.24×10^{-1}
	LSTM	1.98×10^{-3}	3.24×10^{-4}	4.03×10^{-6}	2.01×10^{-3}	1.98×10^{-3}	2.3335	2.00×10^{-1}	1.17×10^{-2}

with 90 % training the proposed model and the remaining 10 % testing its performance. The proposed model takes the elastic deformation portion of the stress-strain plot as input and predicts the values of E, UTS, and FS, thereby avoiding the need for destructive testing. Two models were developed to enhance prediction accuracy. The EUTS-model estimates E and UTS using the elastic deformation dataset as input. In contrast, the FS-model estimates FS using the elastic deformation data and the predicted E and UTS from the EUTS-model.

To develop the EUTS-model and FS-model, various methods, including DT, feedforward NN, and LSTM, were considered. GA-based optimisation techniques were employed to determine the optimal hyperparameters for these methods. Feedforward NN and LSTM were chosen as the best candidates for the feedforward NN model due to their ability to handle complex nonlinear data. A traditional prediction model, DT, was also studied for validation purposes. Several evaluation metrics, such as MSE, CC, R-square, and RMSE, were used to assess the predictive power of the proposed models (optimised DT, LSTM, and feedforward NN). MATLAB functions were utilised to implement the three approaches. The results indicate that the optimised feedforward NN model outperformed the others in predicting UTS and E (EUTS-model). In contrast, the optimised DT model better predicted FS (FS-model).

CRediT authorship contribution statement

Mohammad Reza Chalak Qazani: Investigation, Conceptualization, Resources, Data curation, Methodology, Supervision, Writing – original draft, Funding acquisition, Validation, Writing – review & editing, Formal analysis, Project administration, Software, Visualization. **Mohsen Dorudgar:** Resources. **Mehdi Moayyedian:** Writing – review & editing. **Abdel-Hamid I. Mourad:** Writing – review & editing. **Moosa Sajed:** Investigation, Writing – review & editing, Data curation. **S.M. Hossein Seyedkashi:** Resources, Data curation. **Siamak Pedrammehr:** Writing – review & editing.

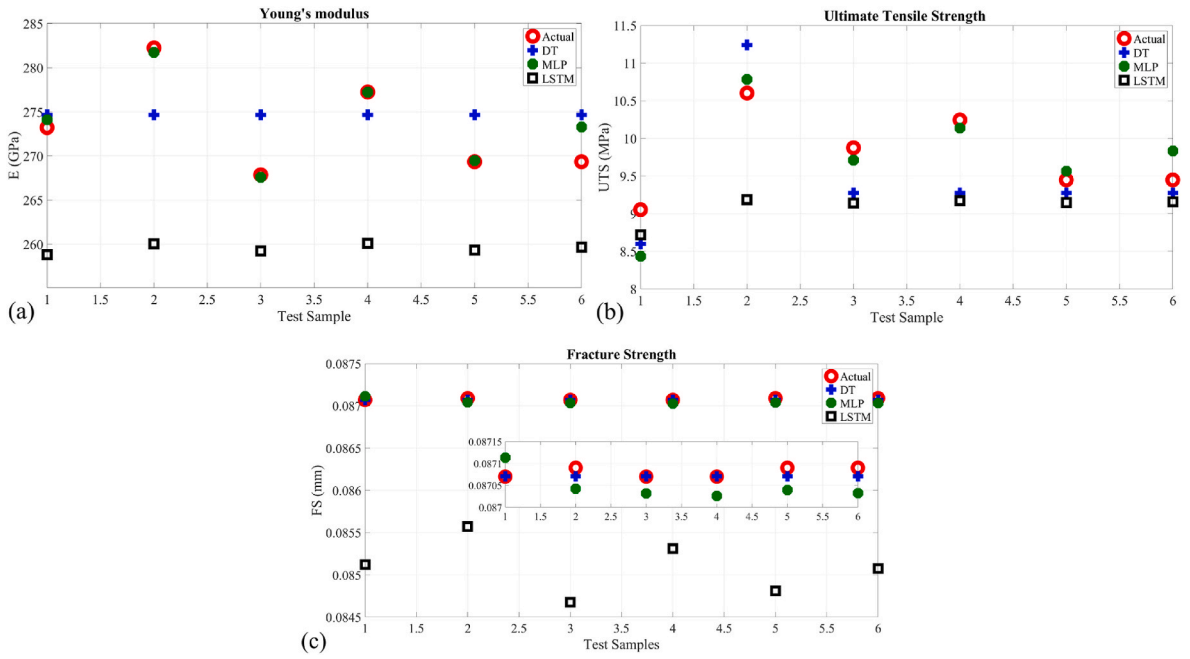

Fig. 8. The actual and predicted values using the optimised model of DT, NN and LSTM for (a): E; (b): UTS; (c): FS.

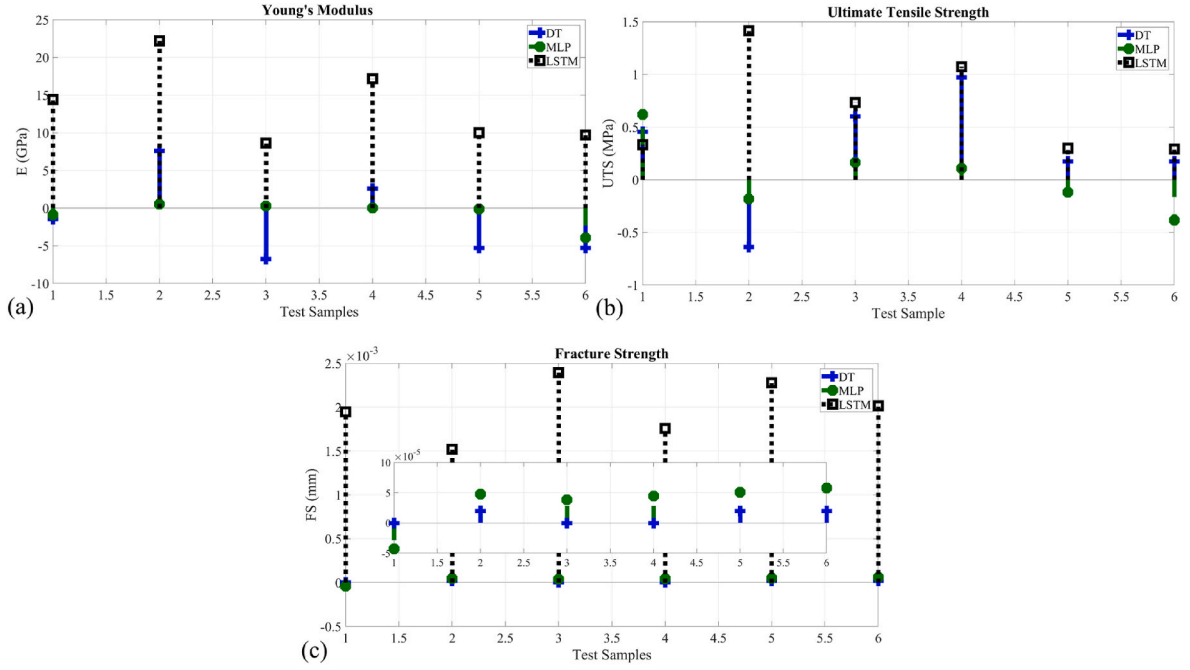

Fig. 9. The error between the actual and predicted values using the optimised model of DT, NN and LSTM for (a): E; (b): UTS; (c): FS.

Declaration of competing interest

The authors declare that they have no known competing financial interests or personal relationships that could have appeared to influence the work reported in this paper.

Data availability

The authors do not have permission to share data.

References

Banhart, J., Seeliger, H.W., 2008. Aluminium foam sandwich panels: manufacture, metallurgy and applications. Adv. Eng. Mater. 10 (9), 793–802.
Banhart, J., Seeliger, H.W., 2012. Recent trends in aluminum foam sandwich technology. Adv. Eng. Mater. 14 (12), 1082–1087.
Brockmann, W., et al., 2009. Adhesive bonding as a joining technique. Adhesive Bonding: Materials, Applications and Technology 1–3.
Dorudgar, M., Seyedkashi, S., Sajed, M., 2021. Experimental study on manufacturing of bi-metal sandwiches with aluminum foam core and copper layers using friction stir welding. Iran. J. Manuf. Eng. 7 (12), 1–9.
Elsheikh, A.H., 2023. Applications of machine learning in friction stir welding: prediction of joint properties, real-time control and tool failure diagnosis. Eng. Appl. Artif. Intell. 121, 105961.

Eren, B., Guvenc, M.A., Mistikoglu, S., 2021. Artificial intelligence applications for friction stir welding: a review. Met. Mater. Int. 27, 193–219.
García-Moreno, F., 2016. Commercial applications of metal foams: their properties and production. Materials 9 (2), 85.
Geiger, M., et al., 2008. Friction stir knead welding of steel aluminium butt joints. Int. J. Mach. Tool Manufact. 48 (5), 515–521.
Ghanbari, S.S., Mahmoudi, A., 2022. An improvement in data interpretation to estimate residual stresses and mechanical properties using instrumented indentation: a comparison between machine learning and Kriging model. Eng. Appl. Artif. Intell. 114, 105186.
Hangai, Y., et al., 2012. Fabrication and tensile tests of aluminum foam sandwich with dense steel face sheets by friction stir processing route. Mater. Trans. 1112261534.
Hangai, Y., et al., 2014. Aluminum alloy foam core sandwich panels fabricated from die casting aluminum alloy by friction stir welding route. J. Mater. Process. Technol. 214 (9), 1928–1934.
Hochreiter, S., Schmidhuber, J., 1997. Long short-term memory. Neural Comput. 9 (8), 1735–1780.
Kadkhodaie Ilkhchi, A., Rezaee, M., Moallemi, S.A., 2006. A fuzzy logic approach for estimation of permeability and rock type from conventional well log data: an example from the Kangan reservoir in the Iran Offshore Gas Field. J. Geophys. Eng. 3 (4), 356–369.
Kruger, G., Eng, B.T.E., 2003. Intelligent monitoring and control system for a friction stir welding process. Signature 20, 1.
Kumar, S., et al., 2023. Prediction of heat generation effect on force torque and mechanical properties at varying tool rotational speed in friction stir welding using Artificial Neural Network. Proc. IME C J. Mech. Eng. Sci., 09544062231155737
Lin, W.-Y., Lee, W.-Y., Hong, T.-P., 2003. Adapting crossover and mutation rates in genetic algorithms. J. Inf. Sci. Eng. 19 (5), 889–903.
Mahmoud, A., et al., 2023. Hydraulic informed multi-layer perceptron for estimating discharge coefficient of labyrinth weir. Eng. Appl. Artif. Intell. 123, 106435.
Marx, J., Rabiei, A., 2021. Tensile properties of composite metal foam and composite metal foam core sandwich panels. J. Sandw. Struct. Mater. 23 (8), 3773–3793.
McCormack, T., et al., 2001. Failure of sandwich beams with metallic foam cores. Int. J. Solid Struct. 38 (28–29), 4901–4920.
Mishra, A., 2020. Artificial intelligence algorithms for the analysis of mechanical property of friction stir welded joints by using python programming. Welding Technology Review 92.
Mishra, A., 2023. Artificial intelligence algorithms for prediction of the ultimate tensile strength of the friction stir welded magnesium alloys. Int. J. Interact. Des. Manuf. 1–9.
Mitchell, M., 1998. An Introduction to Genetic Algorithms. MIT press.
Müssig, J., Graupner, N., 2021. Test methods for Fibre/Matrix adhesion in cellulose fibre-reinforced thermoplastic composite materials: a critical review. Progress in Adhesion and Adhesives 6, 69–130.
Nejad, R.M., et al., 2022. Artificial neural network based fatigue life assessment of friction stir welding AA2024-T351 aluminum alloy and multi-objective optimisation of welding parameters. Int. J. Fatig. 160, 106840.
Nowacki, J., Moraniec, K., 2015. Welding of metallic AlSi foams and AlSi-SiC composite foams. Arch. Civ. Mech. Eng. 15 (4), 940–950.
Okuyucu, H., Kurt, A., Arcaklioglu, E., 2007. Artificial neural network application to the friction stir welding of aluminum plates. Materials & design 28 (1), 78–84.
Ranawat, N.S., et al., 2023. Performance evaluation of LSTM and Bi-LSTM using non-convolutional features for blockage detection in centrifugal pump. Eng. Appl. Artif. Intell. 122, 106092.
Rezaee, M.R., Ilkhchi, A.K., Barabadi, A., 2007. Prediction of shear wave velocity from petrophysical data utilising intelligent systems: an example from a sandstone reservoir of Carnarvon Basin, Australia. J. Petrol. Sci. Eng. 55 (3–4), 201–212.
Rosenblatt, F., 1957. The Perceptron, a Perceiving and Recognising Automaton Project Para. Cornell Aeronautical Laboratory.
Senapati, N.P., Panda, D., Bhoi, R.K., 2021. Prediction of multiple characteristics of Friction-Stir welded joints by Levenberg Marquardt algorithm based artificial neural network. Mater. Today Proc. 41, 391–396.
van Diepen, M., Franses, P.H., 2006. Evaluating chi-squared automatic interaction detection. Inf. Syst. 31 (8), 814–831.
Woo, W., et al., 2008. Grain structure and dislocation density measurements in a friction-stir welded aluminum alloy using X-ray peak profile analysis. Materials Science and Engineering: A 498 (1–2), 308–313.
Wu, C., Wang, C., Kim, J.-W., 2022. Welding sequence optimisation to reduce welding distortion based on coupled artificial neural network and swarm intelligence algorithm. Eng. Appl. Artif. Intell. 114, 105142.
Yang, Y., et al., 2008. Automatic gap detection in friction stir butt welding operations. Int. J. Mach. Tool Manufact. 48 (10), 1161–1169.
Yao, C., et al., 2019. Fabrication and fatigue behavior of aluminum foam sandwich panel via liquid diffusion welding method. Metals 9 (5), 582.
Yousif, Y., Daws, K., Kazem, B., 2008. Prediction of friction stir welding characteristic using neural network. Jordan Journal of Mechanical and Industrial Engineering 2 (3).
Zhang, Z.-j., et al., 2020. Enhanced mechanical performance of brazed sandwich panels with high density square honeycomb-corrugation hybrid cores. Thin-Walled Struct. 151, 106757.